Hindawi Publishing Corporation
International Journal of Distributed Sensor Networks
Volume 2013, Article ID 201767, 12 pages
http://dx.doi.org/10.1155/2013/201767

Research Article

Study on the Stress Relaxation Behavior of Large Diameter B-GFRP Bars Using FBG Sensing Technology

Li Guo-wei,[1,2] Pei Hua-Fu,[3] and Hong Cheng-yu[4]

[1] *Key Laboratory of Ministry of Education for Geomechanics and Embankment Engineering, Hohai University, Nanjing, Jiangsa 210098, China*
[2] *Highway and Railway Engineering Institute, Hohai University, Nanjing, Jiangsu 210098, China*
[3] *Harbin Institute of Technology Shenzhen Graduate School, Department of Civil and Environmental Engineering, Shenzhen 518055, China*
[4] *Department of Civil Engineering, Shantou University, Shantou 515063, China*

Correspondence should be addressed to Pei Hua-Fu; 08902616r@connect.polyu.hk

Received 19 June 2013; Accepted 31 August 2013

Academic Editor: Hong-Nan Li

Corrosion of steel tendons in certain aggressive environments could lead to durability problems of civil engineering. More recently, fiber-reinforced polymer (FRP) rods have been introduced in the market as tendons for prestressed concrete structures because of their lower modulus behavior. However, previous studies on the FRP mechanical time dependent behavior regarding the stress relaxation of large diameter GFRP have not been well understood. This paper investigates the influence of stress levels on the relaxation behavior of a GFRP bar griped with a seamless pipe under sustained deformations ranging from 30% to 60% of its ultimate strain. In order to study the behavior of stress relaxation, two basalt-glass fiber hybrid composite (B-GFRP) bars were developed and instrumented with fiber Bragg grating (FBG) strain sensors. It can be found that the test results reveal that the seamless pipe grip method can undertake 70% of ultimate tensile load of the B-GFRP bar, which can satisfy the requirement of stress relaxation of B-GFRP bar subjected to prestress. The model proposed for evaluating stress relaxation ratio can reflect the influences of the nature of B-GFRP bar and the property of grip method.

1. Introduction

The use of ground anchors has been a common practice in civil and mining engineering. Ground anchors function as temporary or permanent structural members to ensure the stability of various structural systems. In general terms, a grouted anchor is a bar that is inserted and grouted into a hole drilled in rock/concrete. Steel strands and wires have been used as anchor tendons for many years, but in certain aggressive environments, corrosion of steel tendons leads to durability problems [1]. In mainland China, anchor bolt structures were widely used for engineering reinforcement in the 1960s. The problem of low durability in reinforced structures also exists [2]. More recently, fiber-reinforced polymer (FRP) rods have been introduced in the market as tendons for prestressed concrete structures and prestressed ground anchors [3].

Glass FRP (GFRP) bar is the currently available product which is becoming more and more popular in the constructions of concrete structures owing to its low cost compared to CFRP reinforcement. Compared with prestressing steel, the advantages of FRP tendons are (1) high corrosion resistance, (2) high tensile strength, (3) light weight, (4) insensitivity to electromagnetic fields, (5) excellent fatigue behavior, and (6) possible incorporation of optical fiber sensors.

GFRP bar has higher strength and smaller Young's modulus than conventional steel bar [4–6]. The lower modulus of elasticity of an FRP reinforcement may lead to larger deflection of a concrete member after cracking. On the other hand, in prestressed beams, it will lead to a lower loss of

Figure 1: B-GFRP bar used in this study.

prestress due to the shrinkage and creep of concrete [7]. If the FRP bar embedded in reinforced concrete is not pre-stressed, it will not reinforce the structures subjected to slight deformation. Therefore, the prestress is essential for FRP bars used in structural reinforcement.

In the past few decades, the durability of the GFRP materials was recognized as the most critical issue of research. Extensive studies were conducted on the durability of the GFRP material in the 1990s [8–10], including the behavior of GFRP materials and the bond characteristics of GFRP bars in concrete [11–13]. A few studies on time dependent mechanical characteristics of GFRP bars were found in the literature [14–18]. The creep behaviors of GFRP bars obtained from different studies are not consistent such as the review of Laoubi et al. [17] which is different from that of Al-Salloum and Almusallam [18].

For the prestressed or passive FRP ground anchors, reinforced bar produces creep that could cause the stress relaxation. According to the creep behavior of reinforce FRP bar individually, it would be difficult to predict the future stress reduction of the FRP bar subjected to a tensile loading, because its relaxation is related to not only its creep behavior but also the grip method [7]. The grip method of FRP bar is a key technique for pre-stressed FRP reinforced structures. Different grip methods for FRP bars subjected to a tensile force will lead to different slip deformations between the grip body and the FRP bar.

In order to grip the FRP tendons tightly, the methods to grip FRP bar in the structure usually are that (a) the FRP bar was griped on the press with steel pipe anchors [19]; (b) the FRP bar was griped with a steel pipe filled with expansive cement material or paste material [7, 20]; and (c) the FRP bar was griped with a concrete block casted in advance.

Previous research results revealed that a larger diameter GFRP bar has the lower bonding strength than the smaller size [13, 21, 22]. As almost all of the previous researches of GFRP bar durability are for small-sized (diameter less than 20 mm) specimens, the behavior and endurance of larger size GFRP bar are still not well understood, and further research in this aspect is required. Furthermore, ACI 440.1R-01 [23] acknowledged that the creep of GFRP bars and the long-term deflection behavior of concrete members reinforced with FRP need further research to provide information in areas that are still unclear or in need of additional evidence to validate performance.

However, few studies have been conducted on the stress relaxation in GFRP bar. In this paper, the main objective is to examine the effect of stress level on the relaxation behavior of a GFRP bar griped with a seamless pipe under sustained deformations of about 30–60% of its ultimate strain.

2. Experimental Study

The experimental program in this study aims to investigate the effect of stress levels on the relaxation behavior of the GFRP bar griped with a seamless pipe under sustained deformation in laboratory.

2.1. Properties of B-Glass FRP Sand-Coated Bars. The FRP bars used in this study are made of epoxy resin and two types of fibers including basalt and glass fibers. To improve the resistance of pure glass fiber composite to corrosion in alkaline environment, these two types of fibers were used to fabricate a new type of FRP materials. To produce basalt-glass fiber hybrid composites, inner cores of glass fiber are covered by the basalt fibers with better alkali resistance. As shown in Figure 1, the reinforcement materials used in the tests are the basalt-glass fiber hybrid composites with a diameter of 25 mm produced by Zhongshan Pulwell Composites Co., Ltd., in Guangdong Province, China; the basic body is a thermosetting epoxy resin, and the contents of each component (by weight) are resin for 19%, basalt fiber for 10%, glass fiber for 65%, and fine sand for 6%. The mechanical test of the reinforcement material was carried out. The details for physical and mechanical properties of FRP bars used in this study are listed in Tables 1 and 2, respectively.

2.2. Devices for the Stress Relaxation Test of FRP Bar Gripped with Seamless Pipe. If an FRP bar is loaded using traditional wedge-shaped frictional grips, the combination of high compressive stresses and mechanical damage caused by

Figure 2: Centralizer used for fixing FRP bar in the anchorage pipe.

Table 1: Properties of FRP rebars used in this study.

Diameter (mm)		Ratio of fiber weight of basalt to total fiber (%)	Density (g/cm^3)	Content (weight ratio%)			
Basalt	Glass			Basalt	Glass	Resin	Fine sand
2.10	25.35	13.16	2.07	10	65	19	6

Table 2: Properties of FRP rebars.

Item	Calculation method	Value
Ultimate tensile load	$p_{u,\text{ave}}$	536.29 ± 6.74 kN
Ultimate tensile strength	$f_{u,\text{ave}}$	906.40 ± 11.29 MPa
Guaranteed tensile strength	$f_{fu}^* = f_{u,\text{ave}} - 3\sigma$	872.53 MPa
Design tensile strength	$f_{fu} = C_E * f_{fu}^*$, $C_E = 0.7$	610.77 MPa
Modulus of elasticity	$E_{f,\text{ave}}$	52.26 ± 0.87 GPa
Ultimate tensile strain	$\varepsilon_{f,\text{ave}}$	1.73 ± 0.04%
Guaranteed strain	$\varepsilon_u^* = \varepsilon_{u,\text{ave}} - 3\sigma$	1.62%
Design strain	$\varepsilon_u = C_E * \varepsilon_u^*$	1.13%
Allowable strain for creep	20% ε_u	0.23%

the serrations on the wedge surface will lead to premature failure of the grip zone. Griping the FRP bar with a device which could undertake the tensile load for any measurement of mechanical properties is a key technique. In this study, the seamless steel pipe was used to grip the FRP bar by filling the binding agent which could expand by itself to create compressive stress gradually. In order to fix the FRP bar at the centre of grip pipe precisely, the centralizer was designed to keep the FRP bar specimen for the tensile property test, as shown in Figure 2. Firstly, Fix the two half centralizers at the tail tip of the pipe, then put the pipe wrapped with the centralizers vertically, and insert the FRP bar into the pipe until the head of FRP bar crosses through the hole of the centralizers, (Figure 3(a)). Secondly, pour the binding agent liquid into the pipe; the binding agent liquid was made from cement, expansible materials, and water by certain ratio (Figure 3(b)). Thirdly, set up two half centralizers at another end of the pipe, and then put the grip pipe of FRP bar specimen into the water to cure the binding agent for 24 hours (Figure 3(c)). Another end of the specimen was griped as described previously. When all grip actions for FRP bar specimen were ready, these specimens were stored in the normal room temperature (23°C–26°C) and humidity (35%–60%) situation for 28 days, (Figure 3(d)).

The main advantage of this setup is that it can produce a tensile stress that can reach 70% of its ultimate tensile strength for the large diameter FRP bar at the condition of constant deformation. This setup can satisfy the requirements of the durability test of FRP bar simulated to the actual carry processes of pre-stressed structures reinforced with FRP bar. Furthermore, it does not require a large counter weight and large space, and it is easy to operate.

The expansible material chosen was a highly effective soundless cracking agent (HSCA) which was made in the factory of expanding agents of Hezhou city, Guangxi province, China, and it could create a significant expanding force to press the FRP bar body and lead to enough resistant force for preventing the bar body from sliding out of the pipe. The binding agent consisted of cement, HSCA, and water by the weight ratio 0.5 : 0.5 : 0.3.

The principle of anchoring FRP bar inside the seamless pipe is shown in Figure 4(a). A binding agent could expand to create the compressive stress f_{ep} which leads to tensile stress f_T in the pipe wall, Figure 4(b).

(a) Centralizers at the tail tip (b) Centralizers at the mid position (c) Curing in water (d) Curing in chamber

Figure 3: Specimens producing process for FRP bar tensile test.

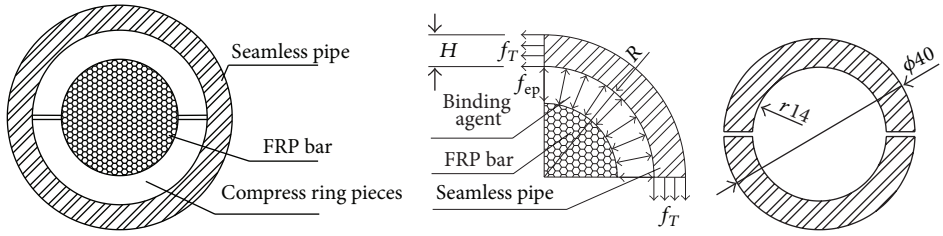

(a) Cross section of anchorage body (b) Mechanical principle (c) Compression ring

Figure 4: Schematic illustration of anchorage pipe of FRP bar specimen for stress relaxation test.

In order to retain the expanding force at the top of the pipe, two compress ring pieces were used to cover on the binding agent and locate between FRP bar and pipe wall, Figure 4(c). Bearing steel plate could stop the ring piece from moving outside during the binding agent expanding and also could close the top binding agent, as shown in Figure 5.

The loading system for the FRP bar relaxation test consisted of hollow jack, bearing plate, load cell, loading pads, and bed plates which could move with the bearing plate during the hollow jack loading, as shown in Figures 6 and 7. The bearing plates could fix the specimen at the suitable position by locking the pipe end of griping pipe in the groove located on the plate, and the optic fiber wires for monitoring could be connected to the outside by crossing the U gap, as shown in Figure 8. When the piston of the hollow jack pushes the bearing plate to move, it could create the space between the bearing plate and the shell of the hollow jack, and then the loading pads are put in the gap to keep the space constant. As shown in Figure 9, corresponding pads were used at different loading stages. The surfaces of pad are smooth enough to keep the load distributing on the bearing plate uniform. Optic fiber Bragg grating (FBG) sensors were installed at the centre of the FRP bar body; FBG sensors were mounted diametrically on the FRP bar.

2.3. Strain Monitoring Method of Fiber Bragg Grating (FBG) Sensors. In the past few decades, structural health monitoring as a key technique for evaluating the performance of geotechnical structures is becoming more and more popular. A variety of instruments including GPS [24, 25] and fiber optic sensors [26] have been widely employed and applied in laboratory tests and engineering projects. The conventional instruments used in the test of the FRP bars include the extensometer, strain gauge, and dial gauge. The test for the FRP bars stress relaxation requires high accuracy, stable signal in long-term monitoring, and small volume suitable for FRP bar. Therefore, conventional instruments cannot satisfy the requirements of the stress relaxation test.

Fiber grating technology is achieved by using the characteristics of the light reflected from grating with a specific wavelength [27]. When the incident light is injected into the fiber, the grating will reflect the light with specific wavelength, the value $\Delta\lambda_B$ of the wavelength shift of this reflected light has linear relationship with the applied strain and temperature changes simultaneously. The wavelength will be changed

Figure 5: Compression ring and location.

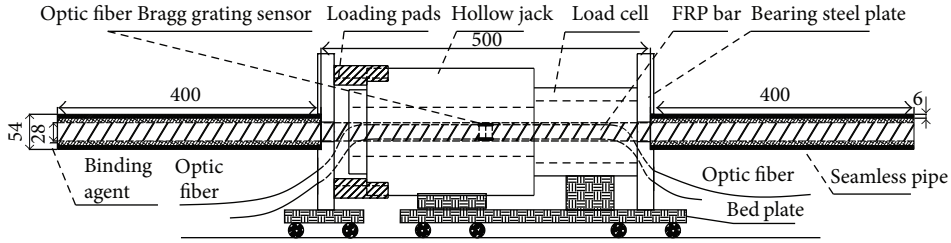

Figure 6: Diagram of the loading system for stress relaxation test.

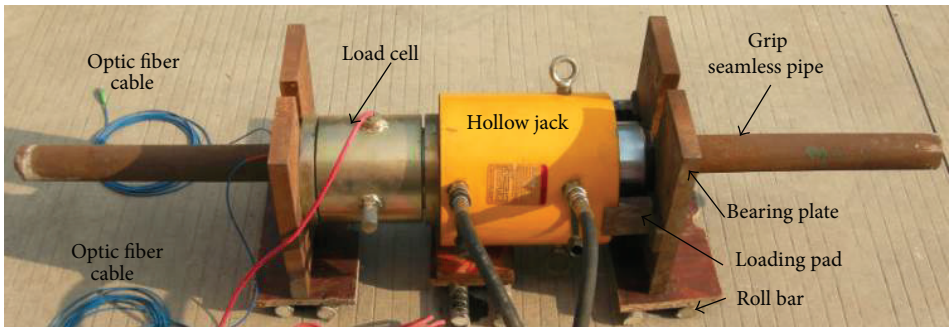

Figure 7: Photo of the loading system for stress relaxation test.

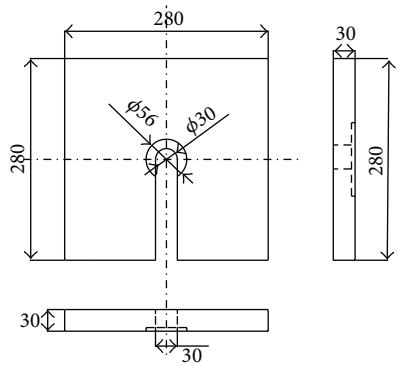

Figure 8: Bearing plate for the tensile loading system.

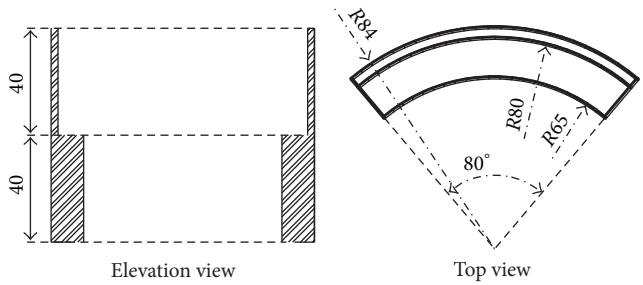

Figure 9: Loading pads.

when the grating is subjected to strain or temperature change. This linear relationship can be expressed as

$$\frac{\Delta\lambda_B}{\lambda_B} = c_\varepsilon \cdot \Delta\varepsilon + c_T \cdot \Delta T, \quad (1)$$

where λ_B is the initial peak wavelength of the reflected light; $\Delta\lambda_B$ is the wavelength shift of peak wavelength; $\Delta\varepsilon$ and ΔT are the strain and temperature, respectively; c_ε and c_T are coefficients for strain and temperature. The main advantages of FBG sensing technology are the clear mechanism of grating sensor and high detection accuracy. Based on the current demodulation technique, the accuracy of fiber grating sensor

Table 3: Summary of relaxation test results for the B-GFRP bar griped with seamless pipes.

Measured data	Phase 1	Phase 2	Phase 3	Phase 4	Phase 5	Phase 6
Max. load stress (MPa)	385.04	425.54	530.42	570.69	649.97	676.13
Ratio of max. load to ultimate strength (%)	42.48	46.95	58.52	62.96	71.71	74.60
Initial stress of relaxation procedure (MPa)	278.17	302.06	365.27	453.34	507.76	Slippage
Ratio of initial stress to ultimate strength (%)	30.69	33.33	40.30	50.02	56.02	Slippage
Initial strain of the centre of bar ($\mu\varepsilon$)	5613.17	5959.42	7316.05	8978.92	10367.79	Slippage
Ratio of initial strain to ultimate strain (%)	32.45	34.45	42.29	51.90	59.93	Slippage
Temperature range (°C)	23.1~25.5	16.8~18.9	15.1~17.8	14.5~18.5	13.5~16.8	/
Period of time (hour)	240	142	206	276	191	/
Modulus of elasticity at loading (GPa)	50.5	51.4	48.7	49.7	50.6	/

(a) Bonding agent loosing (b) Bar slippage (c) State before slipping (d) State after slipping

Figure 10: The damage phenomenon of B-GFRP bar specimen at stress relaxation processes.

in temperature and strain is up to 0.1°C and 1 $\mu\varepsilon$, the data acquisition frequency is up to 5 kHz, and the sensors spacing can be designed and welded according to the test requirements, which can achieve the long-term monitoring.

3. Test Results

In this study, there are many different optimization strategies for sensors distribution [28–30]. Researchers [31–34] conducted a series of GFRP soil nails pullout tests on site. However, the mechanical behavior of GFRP has not been fully investigated in their study. In this experiment, the FBG sensors were uniformly mounted along the tested FRP bars. Based on the strains measured by FBG strain sensors, stress relaxation tests were conducted on two specimens of the B-GFRP bar griped with a seamless pipe at different loading stages in laboratory. The test results were summarized in Table 3.

The load was applied on the specimen by hydraulic jack in stages. To keep the space constant, two specific pads were installed between the bearing plate and the jack shell. The stress and strain at different loading levels were recorded. When the piston returns back, the load applied to the bearing plate decreases immediately and arrives to the initial value of stress because of the gaps being closed. The loading pads were used to fill the space between jack shell and the bearing plate as far as possible to avoid too much loss of stress after unloading. The procedure from the maximum to the initial value of stress for specimen was carried out as fast as possible not more than the actual prestress applying actions period of time. When the initial stress relaxes for a period of time

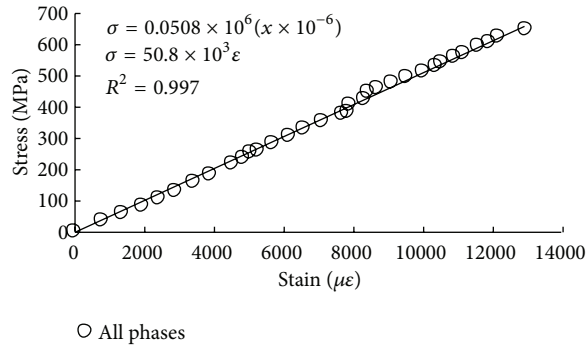

Figure 11: B-GFRP bar Young's modulus in all loading phases.

(approximately 7 days), the rate of stress decreasing becomes smaller, and the trend of stress relaxation appears clearly; it is the time to close the current phase and start the next phase of test.

Six phases of loading were conducted for the specimen, and the related test data were recorded, and some of these were presented in Table 3. The 6th phase only obtained the maximum value of stress because of the B-FRP bar slipping out of the grip pipe during the stress relaxation, as shown in Figure 10.

Test results regarding Young's modulus of B-GFRP bar in all phases, stress relaxation processes, and strain change in every phase are presented in terms of stress versus strain, stress versus elapsed time, and strain versus elapsed time for different conditioning schemes, as shown in Figures 11–14.

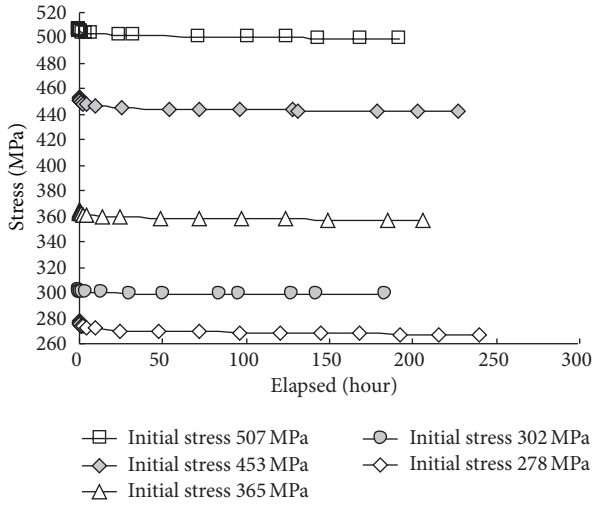

Figure 12: Axial stress of the B-GFRP bar versus elapsed time.

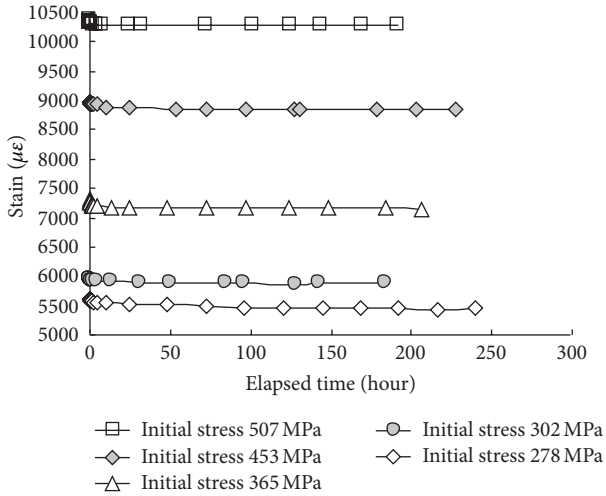

Figure 13: Axial strain of B-GFRP bar versus elapsed time.

4. Analysis of the Behavior of Stress Relaxation

4.1. Behavior of Stress Relaxation of the B-GRP Bar Gripped with a Seamless Pipe. Figure 12 shows that the B-GFRP bar gripped with a seamless pipe has a stress relaxation attribution. In all phases of test, the stress of B-GFRP bar decreases with elapsed time at different rates.

In order to compare the difference of stress relaxation rate of B-GFRP bar subjected to different stress increments at different initial stress levels, the ratio of relaxation for increment of stress was defined as

$$r_{\sigma_i,\Delta\sigma} = \frac{\Delta R_{\Delta\sigma}}{\sigma_i}, \tag{2}$$

where $r_{\sigma_i,\Delta\sigma}$ is the ratio of stress relaxation at a certain initial stress σ_i and a certain stress increment $\Delta\sigma$; $\Delta R_{\Delta\sigma}$ is the variation of stress relaxation at σ_i and $\Delta\sigma$.

Figure 15(a) shows the relationship between the variation of ratio of stress relaxation and elapsed time, which was

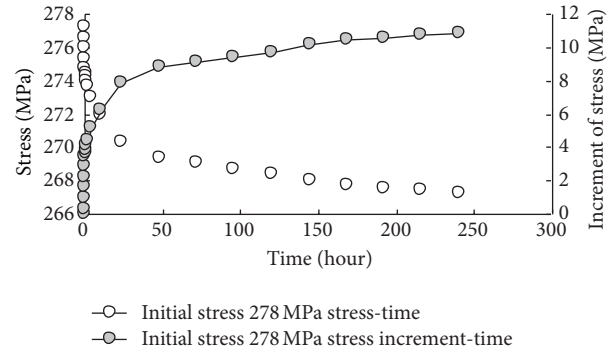

Figure 14: Axial stress deceasing process at an initial stress of 278 MPa.

obtained from all phases tests carried out on the B-GFRP bar specimen gripped with a seamless pipe subjected to a constant deformation. It can be found that the relationship of variation of ratio of stress relaxation and elapsed time is similar to a logarithm curve in every phase which has different initial stress and different stress increments. In order to describe test curves, the horizontal coordinate is shown in logarithmic scale. This change makes the curves straight with different intercepts and slopes, as shown in Figure 15(b). Even though the correlation of model for test data is very high, it is difficult to find a unified linear relationship between the parameters of models and the test conditions.

It should be noticed that the variation of stress relaxation ratio (2) was defined without considering the effect of stress history. It does not consider the quantities of stress relaxation produced in the previous procedure in which the initial stress is less than that of the current. In order to consider the effect of stress history, the definition of variation of stress relaxation is defined as

$$R_{\sigma_i} = R_{\sigma_{i-1}} + \Delta R_{\Delta\sigma}, \tag{3a}$$

$$\sigma_i = \sigma_{i-1} + \Delta\sigma, \tag{3b}$$

where R_{σ_i} is the total variation of stress relaxation at a certain initial stress; $R_{\sigma_{i-1}}$ is the total variation of stress relaxation at a certain initial stress σ_{i-1}; and $\Delta R_{\Delta\sigma}$ is the variation of stress relaxation at a certain increment of stress started at initial stress σ_i.

According to test results, it can be found that

$$\begin{aligned} R_{\sigma_{i-1}} &= A_{\sigma_{i-1}} \cdot \ln(t) + B_{\sigma_{i-1}}, \\ \Delta R_{\Delta\sigma} &= A_{\Delta\sigma} \cdot \ln(t) + B_{\Delta\sigma}, \end{aligned} \tag{4}$$

where $A_{\sigma_{i-1}}$ and $B_{\sigma_{i-1}}$ are the slope and intercept of the straight line of stress relaxation at a previous class of initial stress level, respectively; and $A_{\Delta\sigma}$ and $B_{\Delta\sigma}$ are the slope and intercept of straight line of stress relaxation variation at an increment of stress started at present initial stress, respectively.

Assuming that the procedure of stress relaxation for all phase starts at the same time, (3a) can be expressed as

$$R_{\sigma_i} = A_{\sigma_{i-1}} \cdot \ln(t) + B_{\sigma_{i-1}} + A_{\Delta\sigma} \cdot \ln(t) + B_{\Delta\sigma}. \tag{5}$$

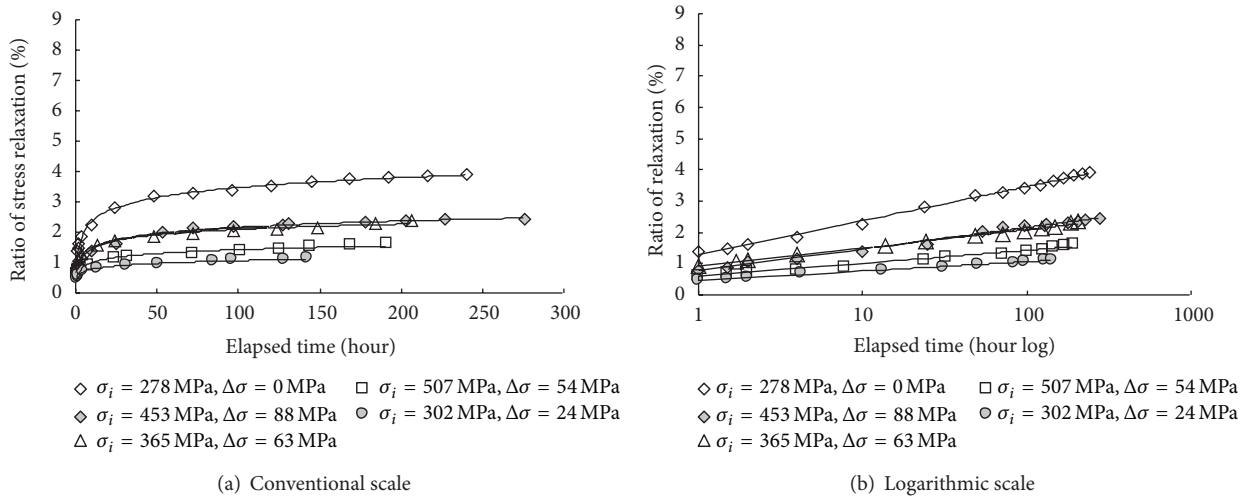

(a) Conventional scale

(b) Logarithmic scale

Figure 15: Ratio of relaxation versus elapsed time.

Table 4: Parameters of stress relaxation variation and ratio for the B-GFRP bar.

Parameters	Phase 1	Phase 2	Phase 3	Phase 4	Phase 5
Initial stress (MPa)	278	302	365	453	507
Increment of stress (MPa)	0	24	63	88	54
Slope of stress relaxation variation, A	1.3025	0.3918	0.8955	1.3887	0.9096
Intercept of stress relaxation variation, B	3.596	1.4041	3.3873	3.4474	2.975
Slope of stress relaxation ratio, a	0.47	0.56	0.71	0.88	0.96
Intercept of stress relaxation ratio, b	1.29	1.66	2.30	2.61	2.92

The accumulated ratio of stress relaxation can be expressed by

$$r_{\sigma_i} = \frac{R_{\sigma_i}}{\sigma_i}, \tag{6}$$

where r_{σ_i} is the accumulated ratio of stress relaxation at initial stress; R_{σ_i} is the accumulated variation of stress relaxation; and σ_i is the initial stress.

Substituting (5) into (6)

$$r_{\sigma_i} = \frac{A_{\sigma_{i-1}} + A_{\Delta\sigma}}{\sigma_i} \cdot \ln(t) + \frac{B_{\sigma_{i-1}} + B_{\Delta\sigma}}{\sigma_i}. \tag{7}$$

By substituting $a_{\sigma_i} = (A_{\sigma_{i-1}} + A_{\Delta\sigma})/\sigma_i$, $b_{\sigma_i} = (B_{\sigma_{i-1}} + B_{\Delta\sigma})/\sigma_i$ to (7), (7) can be expressed by

$$r_{\sigma_i} = a_{\sigma_i} \cdot \ln(t) + b_{\sigma_i}. \tag{8}$$

The test data were reorganized according to (7). Parameters a and b are calculated and listed in Table 4. The stress relaxation ratio curves are plotted in Figure 16(a), and the shape of curves is highly different from before, as shown in Figure 16(a). The straight lines show a clear relationship between slopes and intercepts with initial stress of the relaxation procedure, as shown in Figure 16(b).

It can be found that the slope a_{σ_i} and intercept b_{σ_i} increase with the initial stress simultaneously. The correlation of a_{σ_i} and b_{σ_i} with the initial stress is shown in Figures 17 and 18.

The two parameters of α and β are obtained for the slope by fitting in the relationship about slope and initial stress, as shown in Figure 17. The other two parameters of κ and λ are obtained for the intercept by fitting the relationship between intercepts and initial stress levels, as shown in Figure 18.

Consider

$$\begin{aligned} a_{\sigma_i} &= \alpha \cdot \ln(\sigma_i) + \beta, \\ b_{\sigma_i} &= \kappa \cdot \ln(\sigma_i) + \lambda. \end{aligned} \tag{9}$$

Substituting (9) to (8),

$$r_{\sigma_i} = (\alpha \cdot \ln(\sigma_i) + \beta) \cdot \ln(t) + \kappa \cdot \ln(\sigma_i) + \lambda. \tag{10}$$

Equation (10) is the final unified model describing the stress relaxation procedure of the B-GFRP bar gripped with a seamless pipe, which is obtained from the relaxation test carried out in accordance with step by step loading. α and β all reflect the effect of elapsed time of stress relaxation, which are called delay relaxation parameters. κ and λ reflect the extent of instant relaxation of stress. Thus, they are called instant relaxation parameters.

If $a_{\sigma_i} = 0$, a new parameter σ_{lD} can be obtained. σ_{lD} is the minimum value of the initial stress which can cause delay relaxation of stress, which should be associated with the nature of the B-GFRP bar. Also, if $b_{\sigma_i} = 0$, another parameter σ_{lI} can be obtained, which is the minimum value of initial stress which can cause instant relaxation of stress which should be associated with griping method.

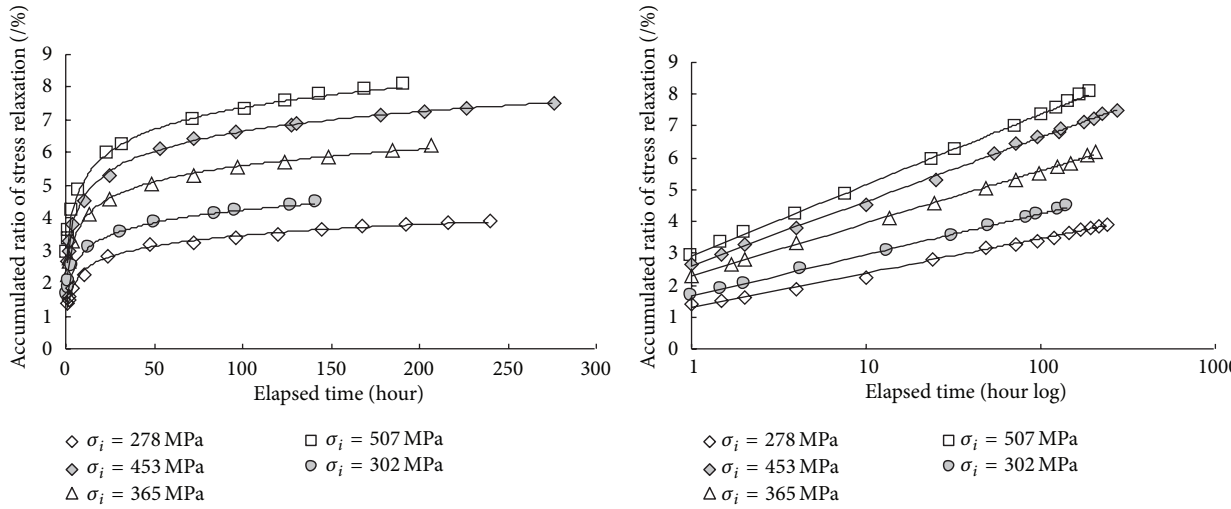

(a) Conventional scale (b) Logarithmic scale

Figure 16: Accumulated ratio of stress relaxation versus elapsed time.

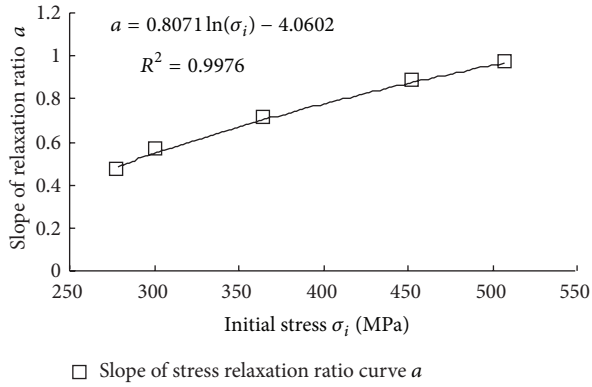

Figure 17: Slopes versus initial stress.

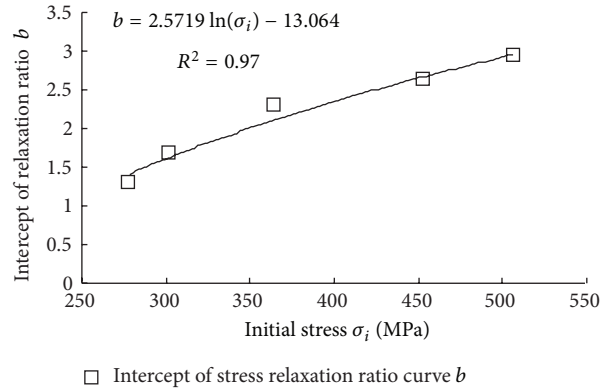

Figure 18: Intercepts versus initial stress.

Consider

$$\sigma_i = \exp\left(-\frac{\beta}{\alpha}\right) = \sigma_{lD},$$
$$\sigma_i = \exp\left(-\frac{\lambda}{\kappa}\right) = \sigma_{lI}. \quad (11)$$

To sum up, six relaxation parameters obtained from the test about the B-GFRP bar gripped with seamless pipe are listed in Table 5. These parameters are substituted into (10) and obtain model curves in Figure 19. It can be found that the model curves fit well with the test curves.

It can be found that a little difference exists between the minimum value σ_{lD} of stress causing delay relaxation and the minimum value σ_{lI} of stress causing instant relaxation, and σ_{lD} is less than σ_{lI}. These test results mean that the procedure of stress relaxation for a B-GFRP bar gripped with seamless pipe can be described precisely by the presented model with 4 parameters, and producing the instant stress relaxation needs larger initial stress relative to the delay relaxation of stress.

Table 5: Parameters of stress relaxation for the B-GFRP bar griped with seamless pipes.

α	β	κ	λ	σ_{lD} (MPa)	σ_{lI} (MPa)
0.81	−4.06	2.57	−13.06	153.03	160.70

Table 6: Ratio of stress relaxation for the B-GFRP soil nail element at a duration of million hours.

Initial stress/ultimate strength		30%	40%	50%	60%	70%
Ratio of stress relaxation at a period of time (%)	10 years	6.81	10.21	12.84	14.99	16.80
	114 years 1,000,000 hours	7.98	11.94	15.01	17.52	19.64

According to the newly developed stress relaxation model, the ratios of stress relaxation in 10 years and one million hours at different initial stress are calculated in Table 6.

4.2. Behavior of Young's Modulus of the B-GFRP Bar in that Procedure of Stress Relaxation. Figure 13 shows that the

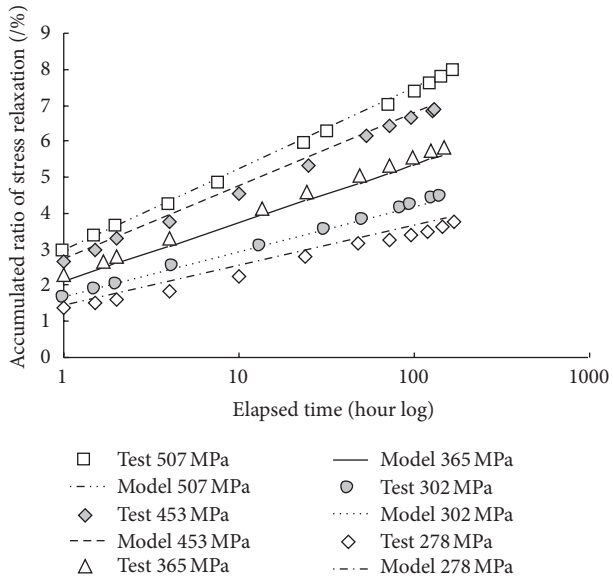

Figure 19: Test curves and model curves of stress relaxation for B-GFRP bars gripped with seamless pipes.

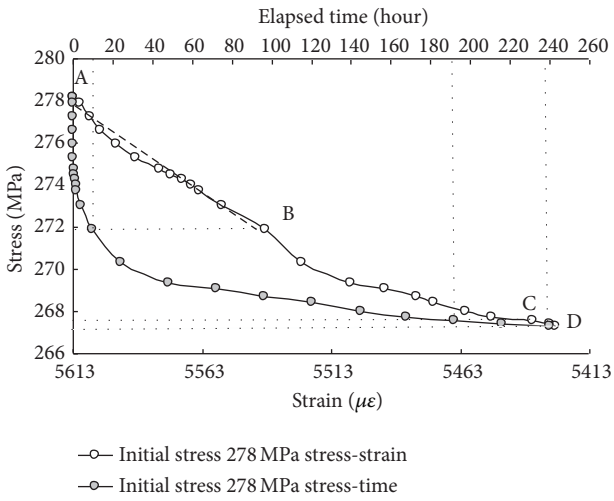

Figure 20: Stress versus strain during stress relaxation process for B-GFRP bar gripped with seamless pipe.

relationship between stress and strain of the B-GFRP bar gripped with a seamless pipe is linear. From these, it can be concluded that the stress relaxation over a long period of time at a lower stress level can not change the slope of linear relationship between stress and strain at a higher stress level for B-GFRP bar. That can be said that the Young's modulus of B-GFRP bar can not be impacted by stress relaxation at lower stress level.

Figure 20 shows the relationship between stress and strain during the stress relaxation for a B-GFRP bar gripped with a seamless pipe. It can be seen that the procedure of stress relaxation can be divided into three periods. In the first period AB, approximately 10 hours, the rate of stress relaxing is very fast and the relationship between stress and strain approaches a straight line. For the second period BC, over a longer time, the rate of stress relaxing becomes slower and the relationship between stress and strain is nonlinear. In the last period CD, the stress and strain change slowly and almost reach a constant value, and the curve approaches a point. Thus, the relationship of stress versus strain of B-GFRP bar is variable during stress relaxation processes, which is a nonlinear relationship and can not be described by a constant modulus.

5. Conclusion

The objectives of this research program are to evaluate the behavior of stress relaxation of a large diameter B-GFRP bar. Two experiments were conducted on the model of stress relaxation of B-GFRP bar in a specialized grip method at different stress levels. Based on the experimental results and analytical studies on sand-coated B-GFRP bar under the described test conditions, the following conclusions can be drawn.

(a) For the large diameter B-GFRP bar (27.45 mm), it can be gripped with seamless pipe by filling a binding agent, which can undertake 70% of its ultimate tensile load. This gripped method can satisfy the requirements for the testing the behavior of stress relaxation of pre-stressed B-GFRP.

(b) The behavior of stress relaxation of B-GFRP bar gripped with seamless pipe subjected to prestress is related to the elapsed time and the initial stress level. A model of stress relaxation ratio was obtained, which has four parameters reflecting the influences of the nature of B-GFRP bar and the property of grip method. It can be concluded that the model is in good agreement with the experimental results.

(c) According to the newly developed stress relaxation model, the ratios of stress relaxation in ten years and one million hours at an initial stress of 30% ultimate strength are 6.81% and 7.98%, respectively.

(d) The stress relaxing over a long period at a lower stress level cannot change the slope of the linear relationship between stress and strain at a higher stress level for the B-GFRP bar.

Acknowledgments

The authors wish to express their gratitude and sincere appreciation for the financial support received from the government of Guangdong province and Ministry of education of China (Project no. 2009B09060011). The help received from the technical staff of the Rock and Soil Mechanics Laboratory in the College of Civil and Transportation Engineering at the Hohai University is also acknowledged.

References

[1] G. H. Koch, M. P. H. Brongers, N. G. Thomson, Y. P. Virmanio, and J. H. Payer, *Cost of Corrosion in the United States, Handbook*

of Environmental Degradation of Materials, William Andrew, Norwich, NY, USA, 2005.

[2] X. Zeng, Z. Chen, J. Wang, and Y. Du, "Research on safety and durability of bolt and cable-supported structures," *Chinese Journal of Rock Mechanics and Engineering*, vol. 23, no. 13, pp. 2235–2242, 2004.

[3] B. Zhang, B. Benmokrane, A. Chennouf, P. Mukhopadhyaya, and A. El-Safty, "Tensile behavior of FRP tendons for prestressed ground anchors," *Journal of Composites for Construction*, vol. 5, no. 2, pp. 85–93, 2001.

[4] G. W. Li, W. M. Ge, C. Ni, J. Dai, and C. L. Mu, "Effect of loading rate on tensile properties of full-scale specimen of larger-diameter glass fiber reinforced polymer (GFRP) bar," *Chinese Journal of Rock Mechanics and Engineering*, vol. 31, no. 7, pp. 1469–1477, 2012.

[5] F. Katsuki and T. Uomoto, "Prediction of deterioration of FRP rods due to alkali attack," in *Proceedings of the 2nd International Conference on Non-Metallic Reinforcement for Concrete Structures*, L. Taewer, Ed., pp. 82–89, (FRPRSC-2), Ghent, Belgium, E&FN SPON, London, UK, 1995.

[6] F. E. Tannous and H. Saadatmanesh, "Durability of AR glass fiber reinforced plastic bars," *Journal of Composites for Construction*, vol. 3, no. 1, pp. 12–19, 1999.

[7] P. X. W. Zou, "Long-term properties and transfer length of fiber-reinforced polymers," *Journal of Composites for Construction*, vol. 7, no. 1, pp. 10–19, 2003.

[8] Y. Chen, J. F. Davalos, I. Ray, and H.-Y. Kim, "Accelerated aging tests for evaluations of durability performance of FRP reinforcing bars for concrete structures," *Composite Structures*, vol. 78, no. 1, pp. 101–111, 2007.

[9] A. S. M. Kamal and M. Boulfiza, "Durability of GFRP rebars in simulated concrete solutions under accelerated aging conditions," *Journal of Composites for Construction*, vol. 15, no. 4, pp. 473–481, 2011.

[10] S. Alsayed, Y. Al-Salloum, T. Almusallam, S. El-Gamal, and M. Aqel, "Performance of glass fiber reinforced polymer bars under elevated temperatures," *Composites B*, vol. 43, no. 5, pp. 2265–2271, 2012.

[11] R. Masmoudi, A. Masmoudi, M. B. Ouezdou, and A. Daoud, "Long-term bond performance of GFRP bars in concrete under temperature ranging from 20°C to 80°C," *Construction and Building Materials*, vol. 25, no. 2, pp. 486–493, 2011.

[12] J. Zhou, X. Chen, and S. Chen, "Durability and service life prediction of GFRP bars embedded in concrete under acid environment," *Nuclear Engineering and Design*, vol. 241, no. 10, pp. 4095–4102, 2011.

[13] J. Alves, A. El-Ragaby, and E. El-Salakawy, "Durability of GFRP bars' bond to concrete under different loading and environmental conditions," *Journal of Composites for Construction*, vol. 15, no. 3, pp. 249–262, 2011.

[14] Z. Wang, O. Joh, and Y. Goto, "Bond creep behavior of FRP rods and their bond strength after sustained loading," *Concrete Engineering Annual Collected Papers*, vol. 21, no. 3, pp. 1513–1518, 1999.

[15] H. Saadatmanesh and F. E. Tannous, "Relaxation, creep, and fatigue behavior of carbon fiber reinforced plastic tendons," *ACI Materials Journal*, vol. 96, no. 2, pp. 143–153, 1999.

[16] B. Benmokrane, P. Wang, T. M. Ton-That, H. Rahman, and J.-F. Robert, "Durability of glass fiber-reinforced polymer reinforcing bars in concrete environment," *Journal of Composites for Construction*, vol. 6, no. 3, pp. 143–153, 2002.

[17] K. Laoubi, E. El-Salakawy, and B. Benmokrane, "Creep and durability of sand-coated glass FRP bars in concrete elements under freeze/thaw cycling and sustained loads," *Cement and Concrete Composites*, vol. 28, no. 10, pp. 869–878, 2006.

[18] Y. A. Al-Salloum and T. H. Almusallam, "Creep effect on the behavior of concrete beams reinforced with GFRP bars subjected to different environments," *Construction and Building Materials*, vol. 21, no. 7, pp. 1510–1519, 2007.

[19] A. Nanni, T. Utsunomiya, H. Yonekura, and M. Tanigaki, "Transmission of prestressing force to concrete by bonded fiber reinforced plastic tendons," *ACI Structural Journal*, vol. 89, no. 3, pp. 335–344, 1992.

[20] D. Schesser, Q. D. Yang, A. Nanni, and J. W. Giancaspro, "Expansive grout-based gripping systems for tensile testing of large diameter composite bars," *Journal of Materials in Civil Engineering*, 2013.

[21] A. Nanni, M. M. Al-Zaharani, S. U. Al-Dulaijan, C. E. Bakis, and T. E. Boothby, "Bond of FRP reinforcement to concrete-Experimental results," in *Proceedings of the 2nd International RILEM Symposium on Nonmetallic FRP Reinforcement for Concrete Structures (FRPRCS-2)*, L. Taerwe, Ed., pp. 135–145, E&FN Spon, Ghent, Belgium, 1995.

[22] B. Benmokrane, B. Tighiouart, and O. Chaallal, "Bond strength and load distribution of composite GFRP reinforcing bars in concrete," *ACI Materials Journal*, vol. 93, no. 3, pp. 246–253, 1996.

[23] A. C. I. Committee 440, *Guide for the Design and Construction of Concrete reinforced with FRP Bars*, ACI 440. 1R-06, American Concrete Institute, Farmington Hills, Mich, USA, 2006.

[24] T.-H. Yi, H.-N. Li, and M. Gu, "Recent research and applications of GPS-based monitoring technology for high-rise structures," *Structural Control and Health Monitoring*, vol. 20, no. 5, pp. 649–670, 2013.

[25] T.-H. Yi, H.-N. Li, and M. Gu, "Characterization and extraction of global positioning system multipath signals using an improved particle-filtering algorithm," *Measurement Science and Technology*, vol. 22, no. 7, Article ID 075101, pp. 1–11, 2011.

[26] H. F. Pei, J. H. Yin, H. H. Zhu, and C. Y. Hong, "Monitoring performance of a glass fiber reinforced polymer soil nail during laboratory pullout test using FBG sensing technique," *International Journal of Geomechanics*, vol. 13, no. 4, pp. 467–472, 2013.

[27] H. F. Pei, J. H. Yin, H. H. Zhu, C. Y. Hong, W. Jin, and D. S. Xu, "Monitoring of lateral displacements of a slope using a series of special FBG based in-place inclinometers," *Measurement Science and Technology*, vol. 23, no. 2, Article ID 025007, 2012.

[28] T.-H. Yi, H.-N. Li, and M. Gu, "A new method for optimal selection of sensor location on a high-rise building using simplified finite element model," *Structural Engineering and Mechanics*, vol. 37, no. 6, pp. 671–684, 2011.

[29] T.-H. Yi, H.-N. Li, and M. Gu, "Optimal sensor placement for structural health monitoring based on multiple optimization strategies," *Structural Design of Tall and Special Buildings*, vol. 20, no. 7, pp. 881–900, 2011.

[30] T. H. Yi, H. N. Li, and X. D. Zhang, "Sensor placement on Canton Tower for health monitoring using asynchronous-climbing monkey algorithm," *Smart Materials and Structures*, vol. 21, no. 12, pp. 1–12, 2012.

[31] H.-H. Zhu, J.-H. Yin, A. T. Yeung, and W. Jin, "Field pullout testing and performance evaluation of GFRP soil nails," *Journal of Geotechnical and Geoenvironmental Engineering*, vol. 137, no. 7, pp. 633–642, 2011.

[32] W.-H. Zhou and J.-H. Yin, "A simple mathematical model for soil nail and soil interaction analysis," *Computers and Geotechnics*, vol. 35, no. 3, pp. 479–488, 2008.

[33] W.-H. Zhou, J.-H. Yin, and C.-Y. Hong, "Finite element modelling of pullout testing on a soil nail in a pullout box under different overburden and grouting pressures," *Canadian Geotechnical Journal*, vol. 48, no. 4, pp. 557–567, 2011.

[34] J.-H. Yin and W.-H. Zhou, "Influence of grouting pressure and overburden stress on the interface resistance of a soil nail," *Journal of Geotechnical and Geoenvironmental Engineering*, vol. 135, no. 9, pp. 1198–1208, 2009.